A Filtering Microstrip Antenna Array

Chin-Kai Lin and Shyh-Jong Chung, *Senior Member, IEEE*

***Abstract*—A new filtering microstrip antenna array is presented. The antenna elements, together with the very compact feeding network, function as a third-order bandpass filter. The feeding network, which consists of one power divider and two baluns, provides the first two stages, and the microstrip antenna elements provide the last stage in the filter design. The equivalent lumped circuit model is analyzed, and the detail synthesis procedure is presented. A third-order filtering 2×2 microstrip antenna array is designed at a center frequency of 5 GHz with 3% fractional bandwidth and Chebyshev 0.3-dB equal-ripple broadside antenna gain response. The results from circuit model, full-wave simulation, and measurements agree well. Compared to the conventional patch antenna array, the proposed filtering microstrip antenna array successfully suppresses the unwanted signals in out-of-band, preserves good selectivity at band edges, and retains the flatness of the passband broadside antenna gain response.**

***Index Terms*—Balun, bandpass filter (BPF), filtering antenna, microstrip antenna array, power divider.**

I. Introduction

As THE development of wireless communication technologies grows rapidly, integration among components has become a significant issue. In a wireless communication system, the antenna is an essential component for receiving and transmitting signals, while the bandpass filter (BPF) is another crucial component for selecting signals in the required band and rejecting the unwanted signals. Generally, a BPF is composed of resonators with the same resonant frequency as the antenna so it leads to interferences on the return loss and the antenna gain responses, especially at the band edges. Usually the impedance bandwidth of the antenna is different from that of the BPF. The I/O ports of a BPF are typically designed for 50-Ω terminations. However, the input impedance of the antenna may not be perfectly matched to 50 Ω at the band edges. The degradation due to mismatch thus occurs. Since both of these components are generally arranged at the very front-end of a communication system, integration of the antenna and the BPF is considered for enhancing the overall performance and reducing circuit area.

Recently, quite a few antennas in different forms were designed through the filter synthesis process, in which the antenna acts as one of the resonators in the filter design. Coupled circular patches were introduced for multiple mode operation in [1]–[4]. Several antennas in different forms, such as slot dipole antennas [5], [6], monopole antennas [7], microstrip antennas [8]–[11], and substrate integrated waveguide (SIW) slot antennas [12] are also integrated with BPFs.

Additionally, over the last few decades, the microstrip antenna array has become one of the most popular candidates for highly directive antenna applications because of its characteristics of low profile, light weight, low cost, and easy fabrication. For the requirement of high directivity, the number of antenna elements tends to increase, and the feeding network must be more complicated. As the feeding network becomes complex, some unexpected resonances occur and result in spurious passbands at unwanted frequencies. Intuitively, the spurious signals can be suppressed by a BPF placed right after the antenna array. However, as mentioned previously, a BPF interacts with the antenna array and degrades the performance, especially at the band edges. In order to solve this dilemma, one of the possible solutions is to replace the antenna elements by the filtering antennas [8]–[11]. If antenna elements act as the first/last stage of the receiver/transmitter have the filtering function, then the signals received/transmitted by the system will no longer be interfered by the noises in unwanted bands.

Traditionally, the feeding network of the antenna array only has the function of transmitting the signals with proper magnitudes and phases to the antenna elements. The feeding network is usually a combination of transmission lines, power dividers, and baluns (balanced-to-unbalanced transformers). Therefore, the filtering power dividers [13] and the filtering baluns [14]–[16] utilizing coupled resonators can be applied for designing the feeding network so that the feeding network has both the functions of power division and band selection.

In this paper, we go a step further by combining the filtering antenna elements and the filtering feeding network so that the circuitry has the return loss and the antenna gain response just like a BPF. A 2×2 antenna array is implemented with a third-order Chebyshev BPF response. Functioning as the last stage of the filter, the radiating patch in [11] is adopted for the array elements, while the feeding network contributes to the first two stages. This paper is organized as follows. Section II illustrates the layout and the equivalent lumped circuit of the filtering microstrip antenna array. Section III describes the design procedure and exhibits the simulation results. Section IV presents the comparison between the proposed filtering microstrip antenna array and nonintegrated conventional patch antenna array with BPF. Section V shows the measured results and is followed by conclusions in Section VI.

II. Structure and Equivalent Circuit

The layout, components, and equivalent circuit of the proposed filtering microstrip antenna array are investigated in this

Manuscript received April 21, 2011; accepted May 02, 2011. Date of publication August 04, 2011; date of current version November 16, 2011. This work was supported in part by the National Science Council, R.O.C., under Contract NSC 97-2221-E-009-041-MY3.

The authors are with the Institute of Communications Engineering, National Chiao Tung University, Hsinchu 300, Taiwan (e-mail: sjchung@cc.nctu.edu.tw).

Color versions of one or more of the figures in this paper are available online at http://ieeexplore.ieee.org.

Digital Object Identifier 10.1109/TMTT.2011.2160986

TABLE I
THIRD-ORDER CHEBYSHEV FILTER PROTOTYPE SPECIFICATIONS

Quantities	Symbols	Values
Order	N	3
Center frequency	f_0	5 GHz
Ripple level	L_A	0.3 dB
Port impedance	Z_0	50 Ω
Fractional bandwidth	Δ	3.0 %

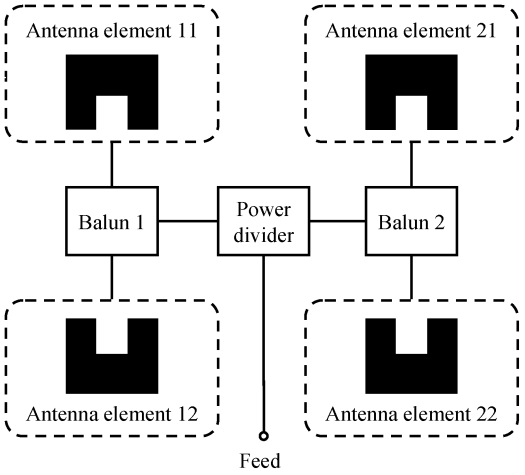

Fig. 1. Functional block diagram of the filtering micristrip antenna array.

section. This design is at a center frequency of 5 GHz, with third-order Chebyshev equal-ripple broadside antenna gain response, 0.3-dB ripple level, 3% fractional bandwidth, and 50-Ω port impedance. The BPF specifications are summarized in Table I.

A. Topology of the Filtering Microstrip Antenna Array

The functional block diagram of the filtering microstrip antenna is illustrated in Fig. 1. At the four corners, four array elements are placed a half free-space wavelength apart from the adjacent ones for minimizing sidelobes. For focusing the main beam in the broadside direction, the feeding network need to be properly designed so that the signals on these four antenna elements are synchronized [17]. The antenna elements 11 and 12 are arranged back to each other for saving the circuit area and reducing the layout complexity. Linked by a balanced- to-unbalanced transformer (balun 1), the antenna elements 11 and 12 have the same phase. The same applies to antenna elements 21 and 22. In order to connect baluns 1 and 2, a power divider is placed at the center to equally split the signal into these two baluns, while the input port of the power divider is connected to the antenna array feeding point.

The physical layout of the proposed filtering microstrip antenna array is depicted in Fig. 2. It is printed on a piece of RT/Duroid 5880 substrate with a dielectric constant of 2.2 and a thickness of 0.508 mm. The filtering microstrip antenna array consists of four parts: four radiating patches, two vertical half-wavelength resonators, one inverted E-shape resonator, and one section of feeding microstrip line with the interdigital coupler.

At the bottom of Fig. 2 is a 50-Ω microstrip feed line of width w_0. At the top end of the feed line is the interdigital coupler for

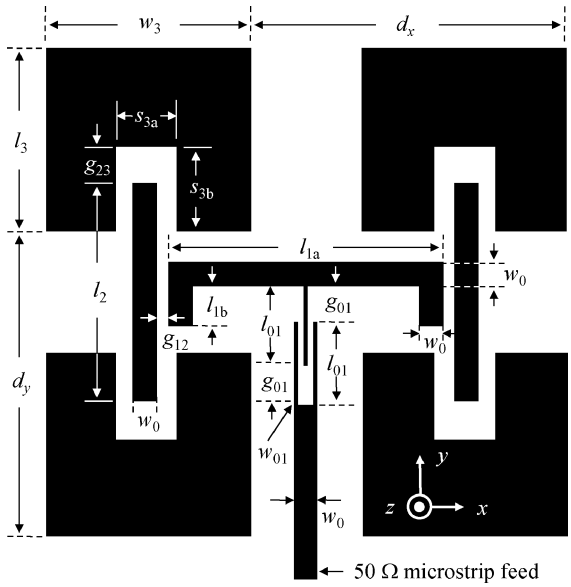

Fig. 2. Topology of the filtering microstrip antenna array.

feeding the first stage, the E-shape resonator. The E-shape resonator is essentially a half-wavelength resonator; $(l_{01}+l_{1a}/2+l_{1b})$ is about half a guiding wavelength. At the sides next to the E-shape resonator, there are two vertical half-wavelength resonators, which act as the second-stage resonators. Since the geometry is symmetrical, the couplings for these two half-wavelength resonators are equal. Thus, the first- and second-stage resonators together can be treated as an equal-power and equal-phase power divider, which corresponds to the power divider in Fig. 1.

Observing the left-hand side of Fig. 2, the half-wavelength resonator and two radiating patches are all operated at their fundamental modes at the same resonant frequency, f_0. Around the resonant frequency, suppose that at some instance in one period, the current flows on the half-wavelength resonator in the $+y$-direction. Through the gap coupling, the current induced on the radiating patches must be in y-direction as well, but with 90° phase difference to the current of the half-wavelength resonator. However, the currents on these two radiating patches are synchronized. Thus, they radiate coherently in broadside ($+z$-) direction. These are the baluns in Fig. 1, which is the similar operation principle inspired by [14]–[16].

On the four corners of Fig. 2, there are four radiating patches as the array elements. The element spacings, d_x and d_y, are both approximately a half free-space wavelength. During the design process, we treat them as the last-stage resonators with loads since they resonate at f_0 and dissipate the electromagnetic power into the air.

B. Equivalent Third-Order BPF Model

Since the filtering microstrip antenna array is composed of coupled resonators, the equivalent circuit in Fig. 3 is constructed accordingly. All the resonators in Fig. 2 are modeled by shunt LC resonators with the same resonant frequency, f_0. The E-shape resonator, the half-wavelength resonators, and the

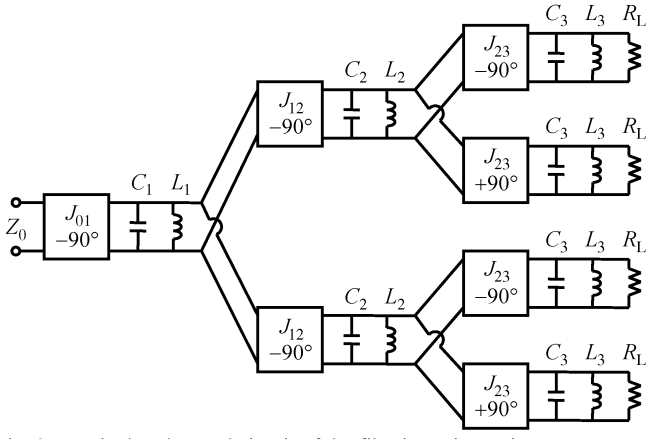

Fig. 3. Equivalent lumped circuit of the filtering microstrip antenna array.

TABLE II
CORRESPONDENCES AMONG FIGURES

Fig. 1. Block diagram	Fig. 2. Physical layout	Fig. 3. Lumped-circuit
Feed	Interdigital coupler	J_{01}
Power divider	E-shape resonator	L_1, C_1, & J_{12}
Balun 1 & 2	Half-wavelength resonator	L_2, C_2, & J_{23}
Antenna elements	U-shape patches	L_3, C_3, & R_L

radiating patches are, respectively, modeled by L_1C_1, L_2C_2, and $L_3C_3R_L$ resonators [17], [18].

The coupling gaps between the resonators are modeled by admittance inverters. The interdigital coupler is modeled by an admittance inverter J_{01}. The coupling between the first and second stages is expressed by two admittance inverters J_{12} with identical -90° phase delay. As for the four gaps between the second and third stages, two of them are modeled by a pair of admittance inverters with -90° phase delay, and the other two are with $+90^\circ$ phase delay. The 180° phase difference among the paired radiating patches are functioning as the baluns. The correspondences among Figs. 1–3 are summarized in Table II.

All of the parameters of the equivalent lumped circuit in Fig. 3 can be calculated utilizing the BPF synthesis technology [18]

$$R_L = Z_0 \tag{1}$$

$$C_1 = \text{arbitrary} \tag{2}$$

$$C_2 = \text{arbitrary} \tag{3}$$

$$C_3 = \frac{g_3}{2\pi f_0 Z_0 \Delta} \tag{4}$$

$$L_i = \frac{1}{4\pi^2 f_0^2 C_i}, \qquad i = 1, 2, 3 \tag{5}$$

$$J_{01} = \sqrt{\frac{\Delta}{g_0 g_1}\frac{2\pi f_0 C_1}{Z_0}} \tag{6}$$

$$J_{12} = \frac{1}{\sqrt{2}} \times 2\pi f_0 \Delta \sqrt{\frac{C_1 C_2}{g_1 g_2}} \tag{7}$$

$$J_{23} = \frac{1}{\sqrt{2}} \times 2\pi f_0 \Delta \sqrt{\frac{C_2 C_3}{g_2 g_3}} \tag{8}$$

where g_0, g_1, g_2, and g_3 are the normalized Chebyshev low-pass filter prototype element values, which are functions of the ripple level L_A. Although C_1 and C_2 have arbitrary values, the first-stage external quality factor (Q_{e1}) and the coupling coefficients between stages (M_{12} and M_{23}) are not affected [18]

$$Q_{e1} = \frac{1}{Z_0 J_{01}^2}\sqrt{\frac{C_1}{L_1}} = \frac{g_0 g_1}{\Delta} \tag{9}$$

$$M_{12} = \sqrt{2} \times \frac{J_{12}}{2\pi f_0 \sqrt{C_1 C_2}} = \frac{\Delta}{g_1 g_2} \tag{10}$$

$$M_{23} = \sqrt{2} \times \frac{J_{23}}{2\pi f_0 \sqrt{C_2 C_3}} = \frac{\Delta}{g_2 g_3}. \tag{11}$$

Note that in (11) and (12), the admittance inverter is slightly different from the ones in conventional filter synthesis. Since power is split into two, the values of the admittance inverters are divided by $\sqrt{2}$.

III. DESIGN

The synthesis of a filtering microstrip antenna array is presented in this section. The filtering microstrip antenna array is deconstructed into several parts, which are designed individually.

By looking up tables in the literature [18], the normalized Chebyshev low-pass filter prototype element values with the ripple level of $L_A = 0.3$ dB are $g_0 = 1.000$, $g_1 = g_3 = 1.371$, and $g_2 = 1.138$. Applying (1)–(11) with the filter specifications given in Table I, the values that we need for parameter extractions are $Q_{e1} = 45.7$, $M_{12} = M_{23} = 0.024$ $R_L = 50\ \Omega$ $C_3 = 29.10$ pF, and $L_3 = 34.82$ pH.

The synthesis of the filtering microstrip antenna array is different from the conventional filter synthesis technologies because the load, or the impedance of port 2 in the filter terminology, cannot be separated from the radiating patch. Therefore, the parameter extractions of the radiating patch, such as external quality factors and the coupling coefficients, are quite different. We are forced to rely more on the lumped circuit model. In the following, the design process will be discussed in detail. The full-wave simulation throughout this work is done using IE3D [19].

A. External Quality Factor of the First-Stage Resonator

Fig. 4 is plotted for designing the feed of the first-stage resonator and the coupling between the first- and second-stage resonators. Fig. 4(a) is the test structure for extracting the external quality factor of the first stage. The thin microstrip section with width w_{01} at the center of the E-shape resonator is for enhancing the coupling with the interdigital coupler [20]. As previously mentioned, $(l_{01} + l_{1a}/2 + l_{1b})$ is about half a guiding wavelength. The dimensions of the E-shape resonator and interdigital coupler in Fig. 4(a) are listed in the figure caption. The coupling gap g_{01} is the tuning variable for the required external quality factor (Q_{e1}) [18]

$$Q_{e1} = \frac{f_0}{\Delta f_{\pm 90^\circ}} \tag{12}$$

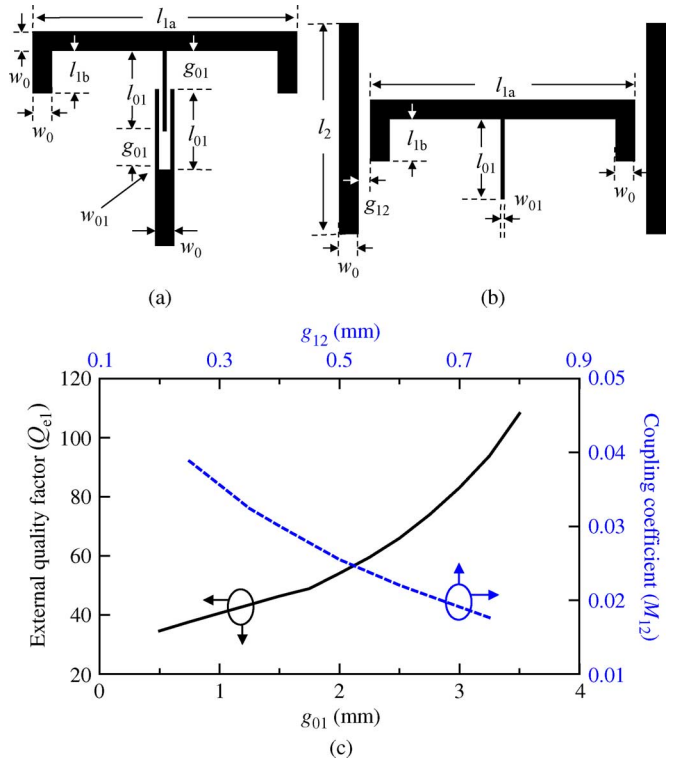

Fig. 4. Q_{e1} and M_{12} extractions. (a) Test structure for the first-stage external quality factor Q_{e1}. The physical dimensions are: $w_0 = 1.15$ mm, $w_{01} = 0.3$ mm, $l_{01} = 0.7$ mm, $l_{1a} = 28.1$ mm, and $l_{1b} = 5.625$ mm, while the gap g_{01} is the tuning variable. (b) Test structure for the coupling coefficient M_{12}. The physical dimensions are: $w_0 = 1.15$ mm, $l_2 = 21.3$ mm, $w_{01} = 0.3$ mm, $l_{01} = 0.7$ mm, $l_{1a} = 28.1$ mm, and $l_{1b} = 5.625$ mm, while the gap g_{12} is the tuning variable. (c) Q_{e1} and M_{12} as the functions of g_{01} and g_{12}, respectively.

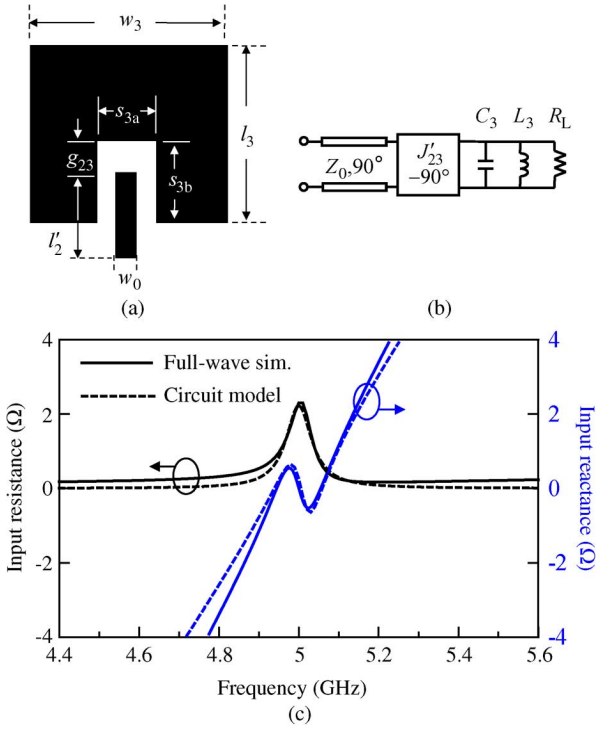

Fig. 5. Radiating patch extraction. (a) Structure under test. (b) Equivalent lumped circuit. (c) Input impedance responses of the full-wave simulated structure and the equivalent lumped circuit with the dimensions $w_3 = 21.0$ mm, $l_3 = 19.3$ mm, $s_{3a} = 5.2$ mm, $s_{3b} = 9.95$ mm, $g_{23} = 4.56$ mm, $l'_2 = 10.65$ mm, and $w_0 = 1.15$ mm.

where f_0 is the resonant frequency and $\Delta f_{\pm 90^\circ}$ is the frequency difference between -90° and $+90^\circ$ of the reflection coefficient. The full-wave simulated Q_{e1} is a function of g_{01} and is plotted in Fig. 4(c). As calculated previously, the required $Q_{e1} = 45.7$. Thus, $g_{01} = 1.7$ mm is chosen for the precise coupling.

B. Coupling Coefficient of the First Two-Stage Resonators

Fig. 4(b) is the structure for testing the coupling between the first two-stage resonators. The first-stage E-shape resonator was already designed in Section III-A. Two 50-Ω half-wavelength resonators with length l_2 and width w_0 are symmetrically placed besides the E-shape resonator with a gap size g_{12}. The dimensions of the structure in Fig. 4(b) are listed in the figure caption.

Using the conventional technique for extracting the coupling between resonators [18], by recording two resonant frequencies of the coupled-resonator structure in Fig. 4(b), f_1 and f_2, then the coupling coefficient between the two resonators, M_{12}, can be calculated

$$M_{12} = \frac{f_2^2 - f_1^2}{f_2^2 + f_1^2}. \tag{13}$$

By adjusting the gap size g_{12}, we can get the proper coupling level. The full-wave simulated M_{12} as a function of g_{12} is plotted (the dashed line) in Fig. 4(c). As calculated previously, the required $M_{12} = 0.024$ and the corresponding gap size $g_{12} = 0.575$ mm should be chosen for the required coupling coefficient.

C. Radiating Patch Design

The radiating patch is modeled by the parallel resonator with three parameters, R_L, L_3, and C_3 to be determined. Since the radiation resistance of the radiating patch is inseparable from the resonator, the conventional external quality factor extraction method for the last stage of the BPF cannot be applied. Instead, we establish the test structure, as shown in Fig. 5(a), for extracting the element values of the corresponding equivalent circuit of the radiating patch in Fig. 5(b).

In Fig. 5(a), the radiating patch is excited by an inserted quarter-wavelength 50-Ω microstrip line with length l'_2, and it is modeled by the $R_L L_3 C_3$ resonator in Fig. 5(b). The coupling between the radiating patch and the quarter-wavelength 50-Ω microstrip line is modeled by an admittance inverter J'_{23}. The coupling here is relatively weaker than that in the final design because the coupling section is not in resonance. That is, J'_{23} is a temporary admittance inverter only for testing and is different from J_{23} in Fig. 3.

These three parameters to be determined $(R_L L_3 C_3)$ correspond to resonant frequency, unloaded quality factor, and load of the resonator [17]. The radiating patch is a half-wavelength square with a coupling section. The resonant frequency of a patch is mainly determined by the patch length l_3. The coupling structure (s_{3a}, s_{3b}) affects the unloaded quality factor. The width of the patch, w_3, mainly affects the antenna resistance R_L, but the unloaded quality factor is also influenced. While the gap

size g_{23} varies, the value of J'_{23} varies. However, the coupling strength does not affect the internal parameters $(R_L L_3 C_3)$ of the resonator.

As shown in Fig. 5(c), the parameters are extracted by fitting the input impedances of the circuits in Fig. 5(a) and (b). The lumped element values that were calculated previously are $C_3 = 29.10$ pF, $L_3 = 34.82$ pH, and $R_L = 50\ \Omega$ The temporary admittance inverter $J'_{23} = 4.1$ mS is obtained by curve fitting. The corresponding dimensions of the radiating patch are listed in the figure caption. From Fig. 5(c), the impedances of the circuit model and full-wave simulation are well fitted.

D. Coupling Between the Last Two-Stage Resonators

Since the radiation resistance of the radiating patch is inseparable from the resonator, once again, the extraction of the coupling between the last two-stage resonators must utilize the equivalent circuit.

Fig. 6(a) depicts the structure under test (one half-wavelength resonator and two radiating patches), and Fig. 6(b) represents its equivalent circuit. The half-wavelength resonator is modeled by L_2C_2. Two radiating patches are modeled by L_3C_3 together with two output ports, port 2 and port 3, with port impedance R_L. The couplings between the last two stages are, respectively, modeled by two admittance inverters, J_{23}, with 180° phase difference, and a loose input coupling is modeled by another admittance inverter with a very small value of J_{test}.

For the equivalent circuit in Fig. 6(b), one of the possible combinations for this previously calculated coupling coefficient $M_{23} = 0.024$ is $C_1 = C_3 = 29.10$ pF, $L_2, = L_3 = 34.82$ pH, and $J_{23} = 14.3$ mS. The normalized S_{21} response (dashed line) of the equivalent circuit is plotted in Fig. 6(c).

The physical dimensions of the radiating patches and the half-wavelength resonator in Fig. 6(a) remain the previously designed values: $w_3 = 21.0$ mm, $l_3 = 19.3$ mm, $s_{3a} = 5.2$ mm, $s_{3b} = 9.95$ mm, $g_{23} = 4.56$ mm, $l_2 = 21.3$ mm, and $w_0 = 1.15$ mm. The half-wavelength resonator is excited by a loose coupled input. Our goal here is to adjust the gap g_{23} to fit the normalized broadside antenna gain response with the normalized S_{21} response of the equivalent circuit. When $g_{23} = 4.56$ mm, as shown in Fig. 6(c), normalized broadside antenna gain response (solid line) fits well with the S_{21} response of the equivalent circuit (dashed line).

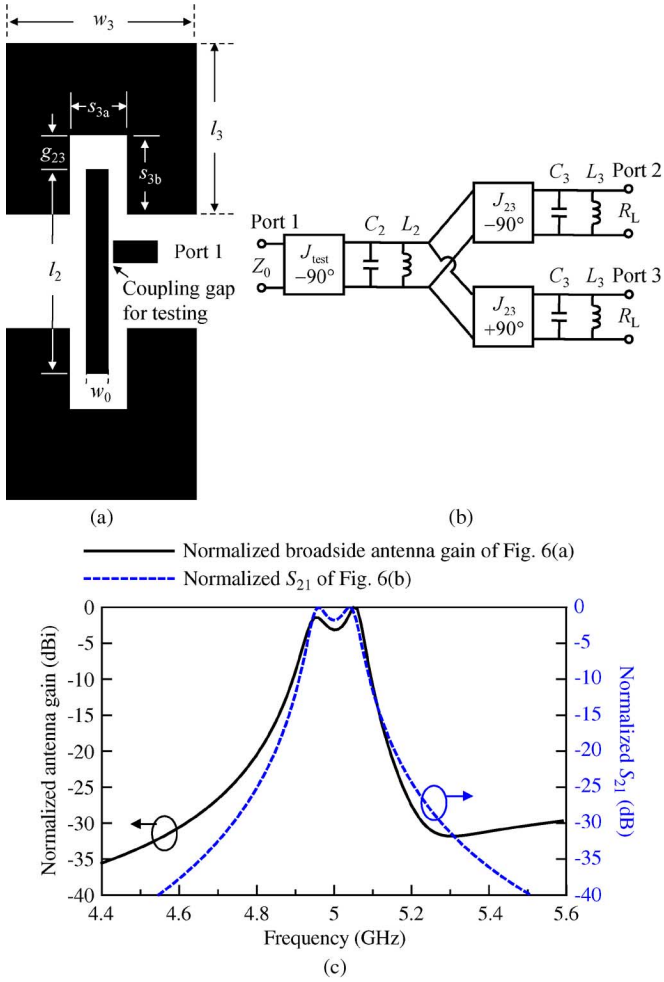

Fig. 6. Extraction of the coupling between the last two stages. (a) Test structure. (b) Equivalent lumped circuit. (c) Comparison of normalized broadside gain and the normalized S_{21} responses with the physical dimensions: $w_3 = 21.0$ mm, $l_3 = 19.3$ mm, $s_{3a} = 5.2$ mm, $s_{3b} = 9.95$ mm, $g_{23} = 4.56$ mm, $l_2 = 21.3$ mm, and $w_0 = 1.15$ mm, and $g_{23} = 4.56$ mm.

E. Simulation Results

After the extraction works, the last step is to put all the stages together. The final dimensions for the filtering microstrip antenna in Fig. 2 are $w_0 = 1.15$ mm, $l_{01} = 0.7$ mm, $w_{01} = 0.3$ mm, $g_{01} = 1.89$ mm, $l_{1a} = 28.1$ mm, $l_{1b} = 5.625$ mm, $g_{12} = 0.575$ mm, $l_2 = 21.3$ mm, $g_{23} = 4.56$ mm, $w_3 = 21.0$ mm, $l_3 = 19.3$ mm, $s_{3a} = 5.2$ mm, and $s_{3b} = 9.95$ mm. The element spacing in x- and y-directions are $d_x = 30.8$ and $d_y = 29.9$ mm, respectively.

Fig. 7 shows the results of both the full-wave simulation and the lumped circuit model. The dashed lines represent the reflection and transmission responses of the lumped circuit model, and the solid lines stand for the full-wave simulated reflection coefficient and the broadside antenna gain responses. The broadside antenna gain of the filtering microstrip antenna array corresponds to the transmission coefficient in the lumped circuit model, in which the antenna resistances, R_L's, are acting as the "remote ports." Both of them are normalized for comparison.

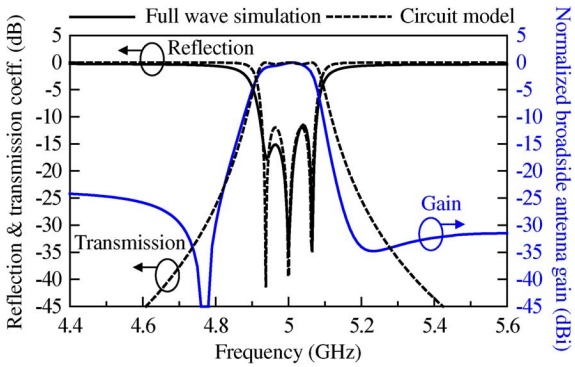

Fig. 7. Simulated reflection coefficients, normalized transmission coefficient, and normalized broadside antenna gain.

Observing the reflection coefficients, the full-wave simulation and the circuit model are in good agreement with minimum

return loss of 11.7 dB and 3% fractional bandwidth (Δ) in the passband.

The filtering microstrip antenna array is symmetric about the yz-plane, which is an H-wall. The cross-polarized component of the broadside (z-) direction antenna gain vanishes for all frequencies. Thus, the broadside antenna gain is purely co-polarized. The maximum value of the co-polarized broadside antenna gain is 9.6 dBi. The out-of-band ($<$4.8 and $>$5.2 GHz) radiation level is -15 dBi or lower. Comparing to the passband antenna gain, a 24-dB rejection is achieved.

Comparing the "broadside antenna gain" and the "transmission mission coefficient" responses, the "broadside antenna gain" has even better selectivity because of the radiation nulls at 4.8 and 5.2 GHz. At these two frequencies, the current induced on the radiating patches are very weak. The radiations due to the open ends of the resonators cancel out each others' contributions in the broadside direction. Around 5.08 GHz, the band edge of the broadside gain response is slightly shifted to lower frequency because the radiation null is close to the passband.

IV. Comparison With a Regular Patch Antenna Array

To demonstrate the advantages of the proposed filtering microstrip array, a conventional patch antenna array and a hairpin BPF are cascaded for comparison.

Fig. 8(a) is the topology that printed on the same substrate, RT/Duroid 5880 with dielectric constant 2.2- and 0.508-mm thickness. Four inset patch antennas are placed a half free-space wavelength (about 30 mm) apart from the adjacent ones. The feeding network is now composed of nonresonant transmission lines and T-junctions. The Chyebyshev hairpin BPF is designed with the same as the specifications listed in Table I. The conventional patch antenna array and the hairpin BPF are interconnected by a section of a 50-Ω microstrip line. The interconnection is *not* optimized because this is the general scenario when we design an RF front end system—components are bridged by 50-Ω transmission lines with arbitrary lengths.

Fig. 8(b) shows the reflection coefficient of the patch antenna array with and without the hairpin BPF. For the patch antenna array without the BPF (dashed line), there is an unexpected spurious radiation at 5.45 GHz. It is caused by the feeding network. This problem can be solved when a BPF is added right after the patch antenna array. However, the antenna resistance is not 50 Ω when the operating frequency is away from its center, while the I/O ports of the BPF are still designed for 50-Ω terminations. The mismatch may lead to the degradation on band-edge selectivity. From the result in Fig. 8(b) (solid line), although the spurious signal at 5.45 GHz is eliminated, there comes an additional resonance at 4.85 GHz due to the interference between the antenna array and the hairpin BPF. In addition, the maximum return loss in pass band is only 6.5 dB at 5.04 GHz, i.e., the passband impedance matching is also degraded.

One of the best ways to solve this problem is to apply the filtering microstrip antenna array. Fig. 8(c) shows the comparison among the broadside antenna gains of several structures. The broadside antenna gain response of the conventional patch antenna array (dashed–dotted line) has a maximum gain of 10 dBi at the center frequency, but with a 2.5-dB gain variation in the passband. For the patch antenna array with the BPF (dashed line), the passband response is seriously affected by the unwanted couplings, and the gain is rather lower than that of the filter microstrip antenna array. For the proposed filtering microstrip antenna array (solid line), although the peak gain is about 1 dB lower, the gain variation reduces to less than 1 dB, the roll-off of the band-edge is much steeper, and the out-of-band rejection is much stronger.

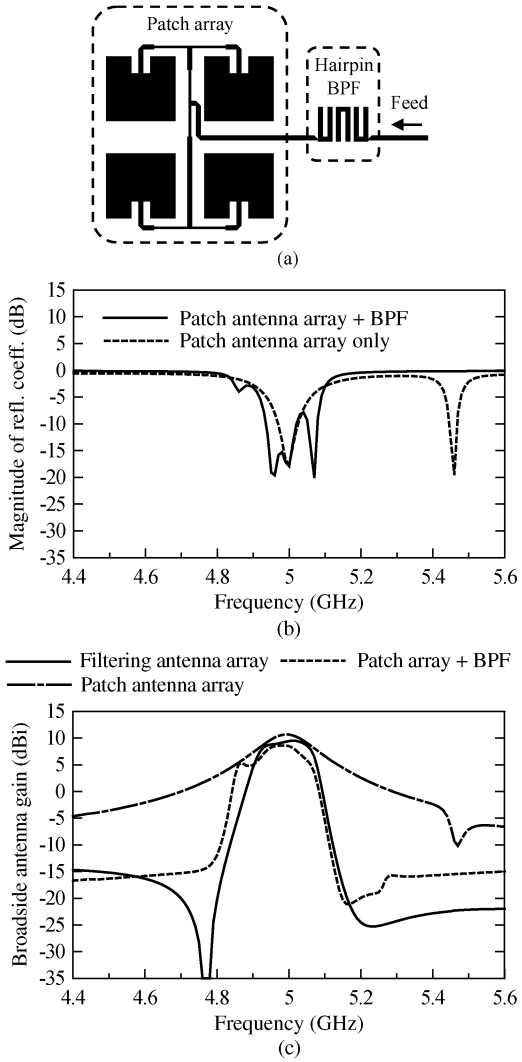

Fig. 8. Comparison between the proposed filtering microstrip antenna and the conventional patch antenna array with/without a hairpin BPF. (a) The conventional patch antenna array and hairpin BPF. (b) Comparison on simulated reflection coefficients. (c) Comparison on simulated broadside antenna gains.

V. Measurement Result

Fig. 9(a)–(c) shows, respectively, the photograph, measured/simulated results, and E-plane radiation patterns of the fabricated filtering microstrip antenna array. In Fig. 9(b), the measured magnitude of reflection coefficient has decent agreement with the simulated gain. In the passband, three transmission poles and minimum return loss of 11.7 dB in the passband are observed, as expected.

The measured co-polarized broadside antenna gain also fits well with the simulated results in passband. In the out-of-band

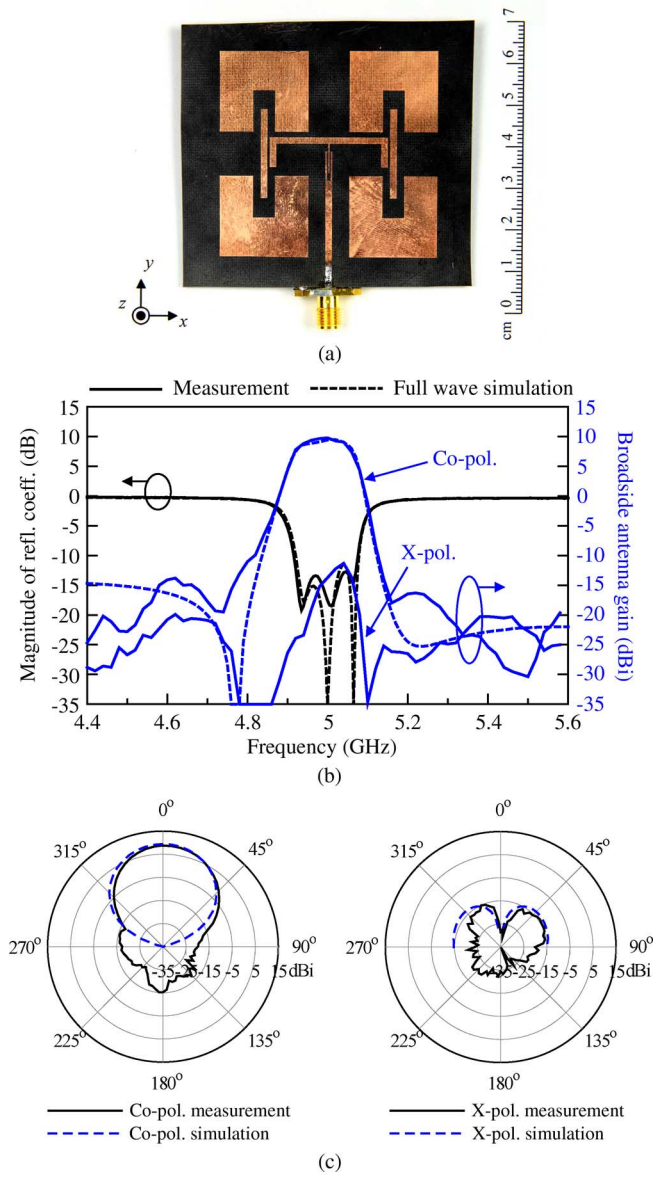

Fig. 9. (a) Photograph of the fabricated filtering microstrip array antenna. (b) Reflection coefficient and broadside antenna gain response. (c) Measured and simulated H-plane (xz-plane) radiation patterns at 5 GHz.

regions, there are some ripples due to the limitation of the sensitivity of the measurement system. However, the out-of-band broadside antenna gain is less than −15 dBi.

As previously mentioned, there is theoretically a cross-polarized radiation null in broadside direction because of geometrical symmetry. The measured cross-polarized gain has a maximum level −12 dBi in the passband due to the measurement error. Nonetheless, this is significantly lower than the co-polarized gain, and can be negligible. The measured antenna efficiency at 5 GHz is 72.2%.

The measured and simulated H-plane radiation patterns at 5 GHz are plotted in Fig. 9(c). Only the upper plane of the simulated radiation pattern is plotted due to the infinite ground setup in IE3D. The radiation pattern of the filtering microstrip antenna array is similar to that of the regular patch antenna array. The co-polarized radiation pattern has a maximum 9.6-dBi gain in broadside direction. The simulated 3-dB beamwidth is 46°. The maximum simulated cross-polarized gain resulted from the resonant structures is about −14 dBi at ±45°. Although the measured broadside cross-polarized radiation null is not so obvious, the radiation level is rather low in all directions.

VI. Conclusion

This paper has presented a third-order filtering microstrip antenna array with a Chebyshev equal-ripple broadside antenna gain response and a pair of antenna nulls beside the passband. Without suffering from any additional circuit area, the antenna elements together with the feeding network own the function of a filter. The detail synthesis procedure and measured results are presented. Comparing to the regular patch antenna array, the proposed filtering microstrip antenna array successfully suppresses the unexpected spurious signals and retains the flatness of the passband broadside antenna gain response.

References

[1] H. Blondeaux, D. Baillargeat, P. Leveque, S. Verdeyme, P. Vaudon, P. Guillon, A. Carlier, and Y. Cailloce, "Microwave device combining and radiating functions for telecommunication satellites," in *IEEE MTT-S Int. Microw. Symp. Dig.*, May 2001, pp. 137–140.

[2] H. Blondeaux, D. Baillareat, S. Verdeyme, P. Guillon, A. Carlier, Y. Cailloce, and E. Rogeaux, "Radiant microwave filter for telecommunications using hi Qu dielectric resonator," in *Proc. 30th Eur. Microw. Conf.*, 2000, pp. 1–4.

[3] I. Hunter, "Broadband matching of antenna using dual-mode radiators," in *Proc. 33rd Eur. Microw. Conf.*, 2003, pp. 431–434.

[4] A. I. Abunjaileh, I. C. Hunter, and A. H. Kemp, "A circuit-theoretic approach to the design of quadruple-mode broadband microstrip antennas," *IEEE Trans. Microw. Theory Tech.*, vol. 56, no. 4, pp. 896–900, Apr. 2008.

[5] S. Oda, S. Sakaguchi, H. Kanaya, R. K. Pokharel, and K. Yoshida, "Electrically small superconducting antennas with bandpass filters," *IEEE Trans. Appl. Supercond.*, vol. 17, no. 2, pp. 878–881, Jun. 2007.

[6] T. E. Nadan, J. P. Coupez, S. Toutain, and C. Person, "Integration of an antenna/filter device, using a multi-layer, multi-technology process," in *Proc. 28th Eur. Microw. Conf.*, 1998, pp. 672–677.

[7] C.-T. Chuang and S.-J. Chung, "New printed filtering antenna with selectivity enhancement," in *Proc. 39th Eur. Microw. Conf.*, 2009, pp. 747–750.

[8] T. L. Nadan, J. P. Coupez, S. Toutain, and C. Person, "Optimization and miniaturization of a filter/antenna multi-function module using a composite ceramic-foam substrate," in *IEEE MTT-S Int. Microw. Symp. Dig.*, Jun. 1999, pp. 219–222.

[9] A. Abbaspour-Tamijani, J. Rizk, and G. Rebeiz, "Integration of filters and microstrip antennas," in *Proc. IEEE AP-S Int. Symp.*, Jun. 2002, pp. 874–877.

[10] F. Queudet, I. Pele, B. Froppier, Y. Mahe, and S. Toutain, "Integration of pass-band filters in patch antennas," in *Proc. 32th Eur. Microw. Conf.*, 2002, pp. 685–688.

[11] C.-K. Lin and S.-J. Chung, "A compact edge-fed filtering microstrip antenna with 0.2 dB equal-ripple response," in *Proc. 39th Eur. Microw. Conf.*, 2009, pp. 378–380.

[12] S. Avrillon, I. Pele, A. Chousseaud, and S. Toutain, "Dual-band power divider based on semiloop stepped-impedance resonators," *IEEE Trans. Microw. Theory Tech.*, vol. 51, no. 4, pp. 1269–1273, Apr. 2003.

[13] Y. Yusuf and X. Gong, "A new class of 3-D filter/antenna integration with high quality factor and high efficiency," in *IEEE MTT-S Int. Microw. Symp. Dig.*, May 2010, pp. 892–895.

[14] K.-T. Chen and S.-J. Chung, "A novel compact balanced-to-unbalanced low-temperature co-fired ceramic bandpass filter with three coupled lines configuration," *IEEE Trans. Microw. Theory Tech.*, vol. 56, no. 7, pp. 1714–1720, Jul. 2008.

[15] C.-H. Wu, C.-H. Wang, S.-Y. Chen, and C.-H. Chen, "Balanced-to-unbalanced bandpass filters and the antenna application," *IEEE Trans. Microw. Theory Tech.*, vol. 56, no. 11, pp. 2474–2482, Nov. 2008.

[16] L. K. Yeung and K. L. Wu, "A dual-band coupled-line balun filter," *IEEE Trans. Microw. Theory Tech.*, vol. 55, no. 11, pp. 2406–2411, Nov. 2007.
[17] C. A. Balanis, *Antenna Theory*, 2nd ed. New York: Wiley, 1997, ch. 14.
[18] J. S. Hong and M. J. Lancaster, *Microstrip Filters for RF/Microwave Applications*. New York: Wiley, 2001.
[19] S. W. Wong and L. Zhu, "Implementation of compact UWB bandpass filter with a notch-band," *IEEE Microw. Wireless Compon. Lett.*, vol. 18, no. 1, pp. 10–12, Jan. 2008.
[20] IE3D Simulator. Zeland Softw. Inc., Fremont, CA, Jan. 1997.

Chin-Kai Lin was born in Keelung, Taiwan. He received the B.S. and M.S. degree in physics from National Tsing Hua University, Hsinchu, Taiwan, in 2004 and 2006, respectively, and is currently working toward the Ph.D. degree in communication engineering at National Chiao Tung University, Hsinchu, Taiwan.

His current research interests include the design of antennas and microwave circuits.

Shyh-Jong Chung (M'92–SM'06) was born in Taipei, Taiwan. He received the B.S.E.E. and Ph.D. degrees from National Taiwan University, Taipei, Taiwan, in 1984 and 1988, respectively.

Since 1988, he has been with the Department of Communication Engineering, National Chiao Tung University, Hsinchu, Taiwan, where he is currently a Professor. From September 1995 to August 1996, he was a Visiting Scholar with the Department of Electrical Engineering, Texas, A&M University, College Station. His areas of interest include the design and applications of active and passive planar antennas, low-temperature co-fired ceramic (LTCC)-based RF components and modules, packaging effects of microwave circuits, vehicle collision warning radars, and communications in intelligent transportation systems (ITSs).

Dr. Chung was the treasurer of the IEEE Taipei Section (2001–2003) and the chairman of the IEEE Microwave Theory and Techniques Society (IEEE MTT-S) Taipei Chapter (2005–2006). He was the recipient of the Outstanding Electrical Engineering Professor Award of the Chinese Institute of Electrical Engineering and the Teaching Excellence Awards of the National Chiao Tung University (both in 2005).